Supplementary Information

Structural Interactions in Polymer Stabilized Magnetic Nanocomposites

*Gauri M. Nabar[⊥,‡], Abhilasha V. Dehankar[⊥,‡], Elizabeth Jergens[⊥], Benworth B. Hansen[⊥], Ezekiel Johnston-Halperin[§], Matthew Sheffield[§], Joshua Sangoro[⊥], Barbara E. Wyslouzil[⊥,∥], Jessica O. Winter[⊥,†,]**

[⊥] William G. Lowrie Department of Chemical and Biomolecular Engineering, The Ohio State University, 151 W. Woodruff Ave. Columbus, OH 43210, USA.

[§] Department of Physics, The Ohio State University, Columbus, Ohio 43210, USA

[∥] Department of Chemistry and Biochemistry, The Ohio State University, 151 W. Woodruff Ave., Columbus, OH 43210, USA

[†] Department of Biomedical Engineering, The Ohio State University, 151 W. Woodruff Ave. Columbus, OH 43210, USA

*Corresponding author: Electronic mail: winter.63@osu.edu

[‡] Gauri M. Nabar and Abhilasha V. Dehankar contributed equally to this work.

Portions of this material were published in the PhD thesis of Gauri M. Nabar[1] and are cited where appropriate.

Supplementary Figures 1-2

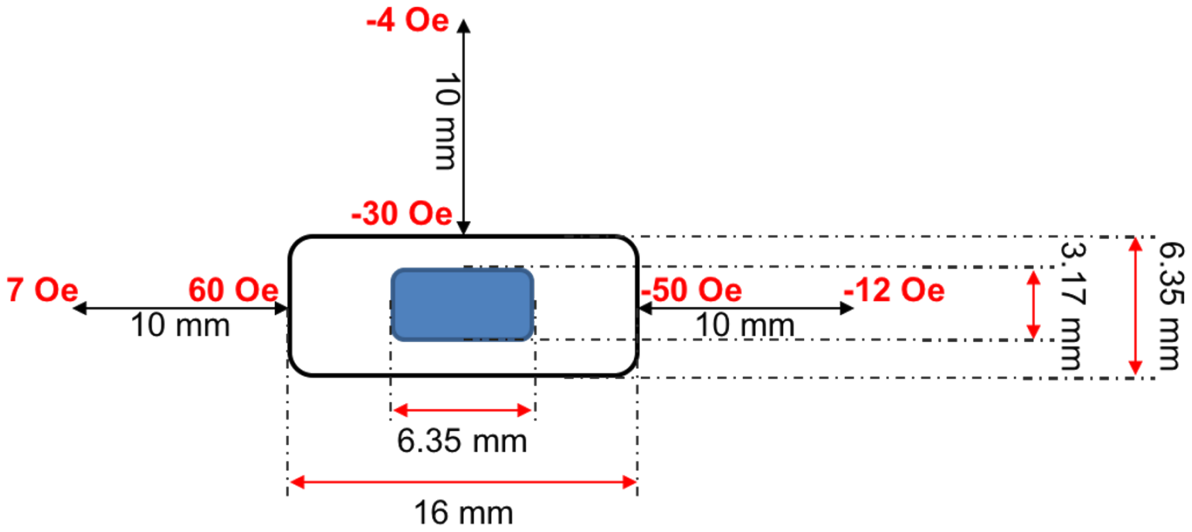

Supplementary Figure 1: Stir bar magnetic field as measured using a handheld magnetometer placed at varying locations and distances from the surface.

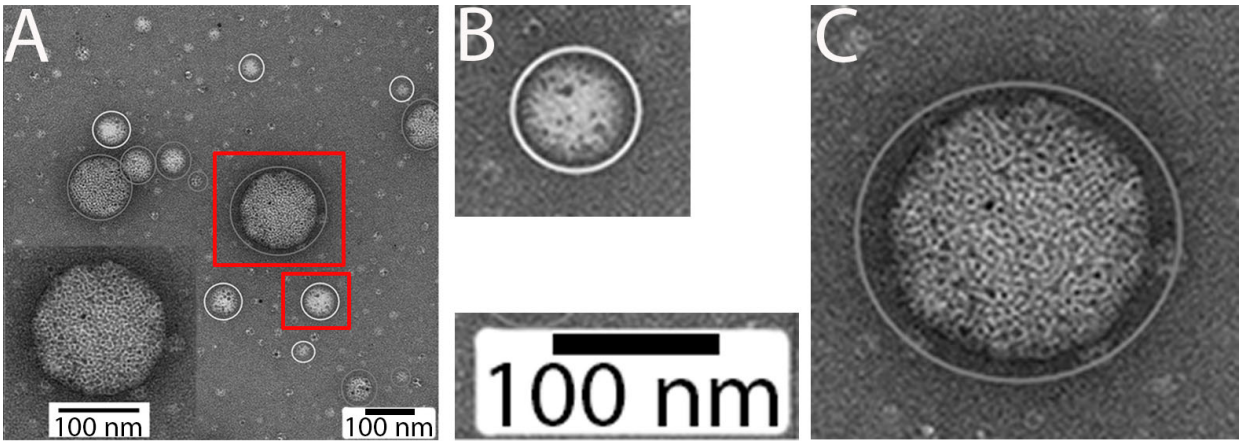

Supplementary Figure 2: Examples of SPION micelle and aggregate SPION nanocomposites (SNC)s. (A) Original panel of Figure 2 in the main manuscript. Red boxes show example particles that have been enlarged. (B) Example SPION micelle from panel A. SPION micelles are characterized by smaller sizes and large amounts of white space in the micelle interior. (C) Example SNC. SNCs are characterized by larger sizes and filling of the micelle interior with SPIONs.

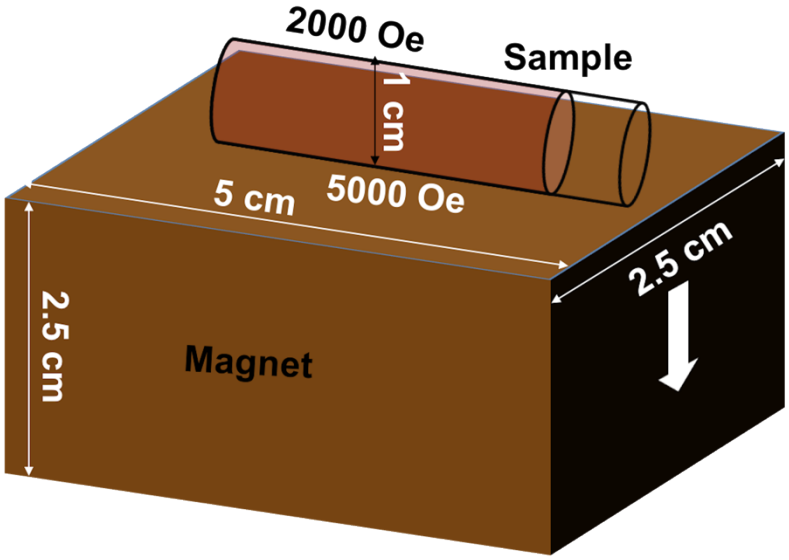

Supplementary Figure 3: Magnetic field of a neodymium magnet applied post-synthesis as measured using a handheld magnetometer at varying locations and distances from the surface.

Supplementary Results and Discussion (including Supplementary Figure 4-5)[1]

Polymer Bridges

Post-synthesis magnetic field exposure occasionally led to structure aggregation (Supplementary Figure 4), including the formation of polymer bridges (circled, Supplementary Figure 4). These structures were only observed in samples exposed to magnetic fields, indicating field application plays a role in their formation. The presence of these large aggregates may alter expected vehicle performance in their intended applications and must be thoroughly investigated. In our system, aggregation could occur by one of two possible routes. First, organic solvent may be present in solution or structures post-synthesis. As structures are enriched by magnetic concentration, they may come into contact and fuse because of BCP or polyvinyl alcohol (PVA) surfactant chain mobility imparted by the residual solvent. Alternatively, aggregation could also be induced by dipole coupling facilitated by application of external fields to overcome thermal fluctuations.

Densely loaded aggregates would experience dipole attractions proportional to cluster size[2]. If dipole interactions are strong, they may be sufficient to overcome the glassy nature of the BCP polystyrene (PS) block, permitting structure aggregation and merging to form the irregularly shaped aggregates and the polymer bridges observed in Supplementary Figure 4.

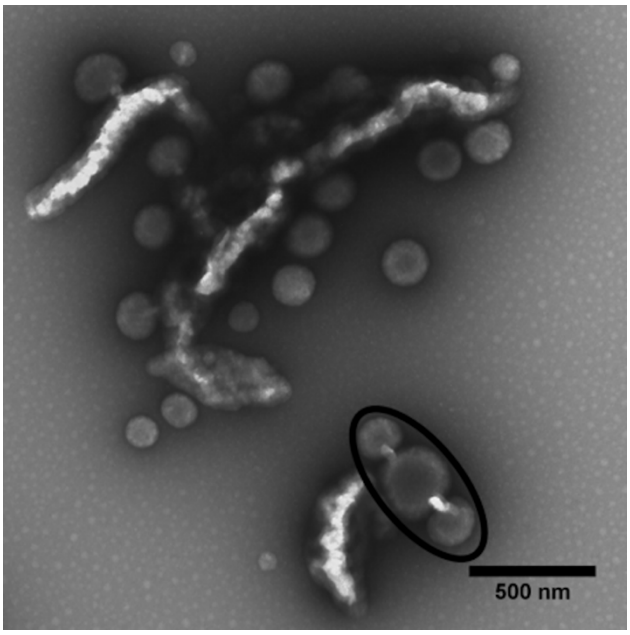

Supplementary Figure 4: Aggregation of densely loaded SPION aggregates observed in the presence of magnetic fields. Black circle indicates structures connected by polymer bridges. Scale bar = 500 nm.

Polymeric filamentous structures

In addition to polymer bridges, polymer filaments were also observed in the presence of applied magnetic fields. Filaments displayed mean widths of 11.4 ± 1.2 nm (Supplementary Figure 5A) and did not contain SPIONs. We hypothesized three possible compositions for these structures: (1) PS-b-polyethylene oxide (PEO) BCP wormlike micelles (WLMs), (2) hybrids comprised of PS-b-PEO and PVA surfactant, or (3) fibers comprised of PVA. As we did not observe spherical endcaps indicative of WLMs and diameters were smaller than those reported by PS-b-PEO WLMs, we do not believe that the fibers are WLMs. We also discount the second possibility of a hybrid

structures, as we have also seen similar structures when preparing SPION nanocomposites using PVA in the absence of PS-b-PEO (Supplementary Figure 5B). Thus, we conclude these filaments are most likely comprised of PVA. Similar PVA fibers have been reported in electrospinning syntheses[3]. It is surprising that PVA fibers were produced using the interfacial instability process, which allows the system to slowly come to equilibrium. This finding should be further investigated. Given their lack of inherent magnetism, these structures would not be expected to be collected from solution with magnetic exposure. We hypothesize that densely loaded aggregates were likely entangled in PVA fibers, permitting their collection by a magnet.

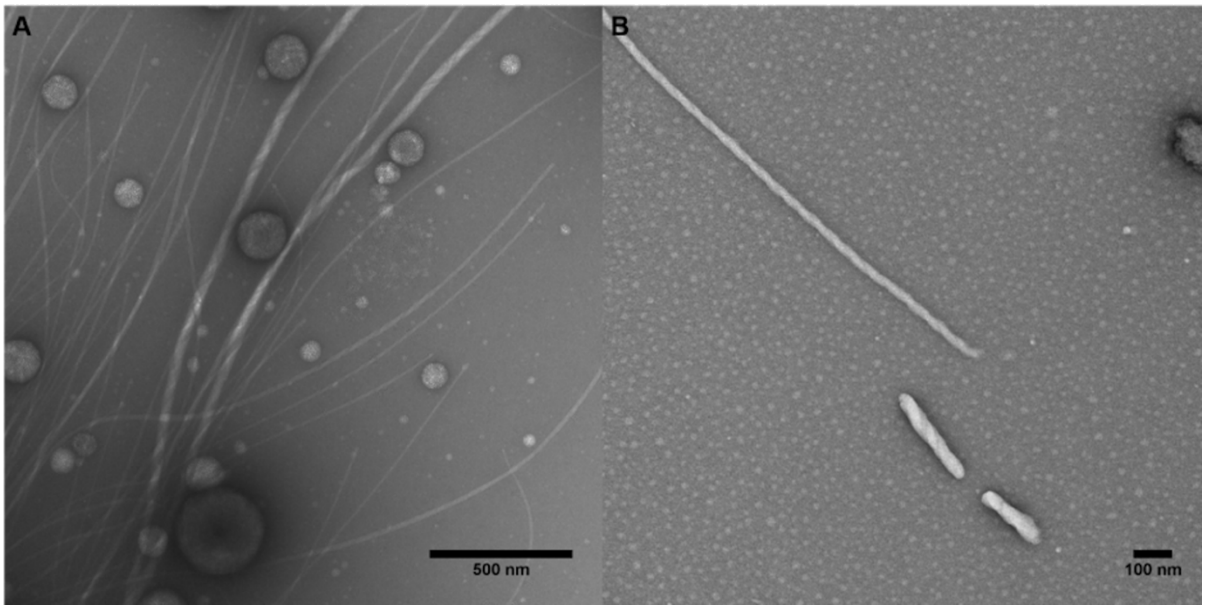

Supplementary Figure 5: Polymer filaments observed in (A) the magnetically concentrated pellet and (B) similar structures generated by interfacial instability with SPIONs and PVA only (no PS-b-PEO BCP).

Supplementary Figures 6-12

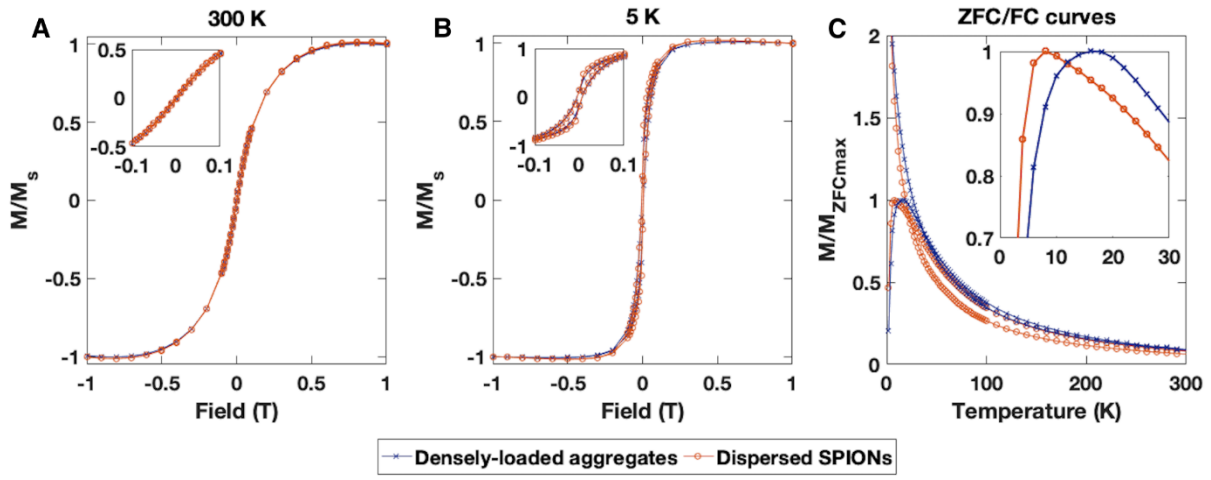

Supplementary Figure 6: Magnetization curves for dispersed SPIONs (orange) and densely loaded aggregates with no magnetic field exposure (blue) at (A) 300 K with field sweep, Inset: -0.1 T < Field < 0.1 T; (B) 5 K with field sweep, Inset: -0.1 T < Field < 0.1 T; and corresponding (C) ZFC/FC curves measured at zero and 5T fields, respectively, Inset: 0-30 K. Note that in A, B curves for dispersed SPIONs and densely loaded aggregates nearly completely overlap, obscuring the blue aggregate curve (magnified in Supplementary Figure 7).

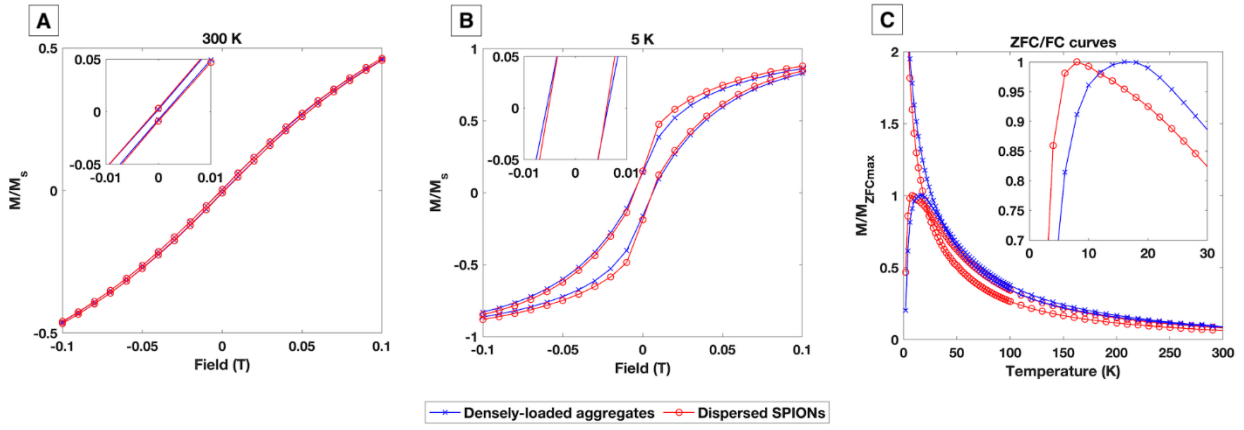

Supplementary Figure 7: Magnetization curves for dispersed SPIONs (red) and densely-loaded aggregates (blue) with no other field exposure at (A) 300 K with field sweep -100 Oe < Field < 100 Oe, Inset: -0.1 T < Field < 0.1 T; (B) 5 K with field sweep -100 Oe < Field < 100 Oe, Inset: -0.1 T < Field < 0.1 T; and corresponding (C) ZFC/FC curves measured at zero and 5T fields, respectively, Inset: 0-30 K.

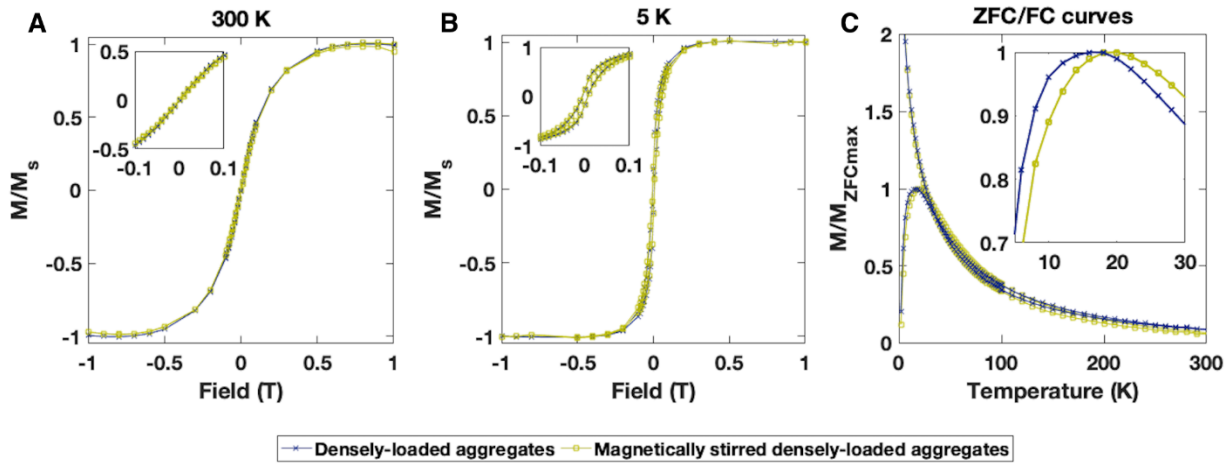

Supplementary Figure 8: Magnetization curves for densely loaded aggregates (blue) and magnetically-stirred aggregates (green) at (A) 300 K field sweep, Inset: -0.1 T < Field < 0.1 T; (B) 5 K field sweep, Inset: -0.1 T < Field < 0.1 T; and (C) corresponding ZFC/FC curves measured at zero and 5T fields, respectively, Inset: 0-30 K. Note that in A, B curves for densely loaded aggregates and magnetically-stirred densely loaded aggregates nearly completely overlap, obscuring the blue aggregate curve (magnified in Supplementary Figure 9).

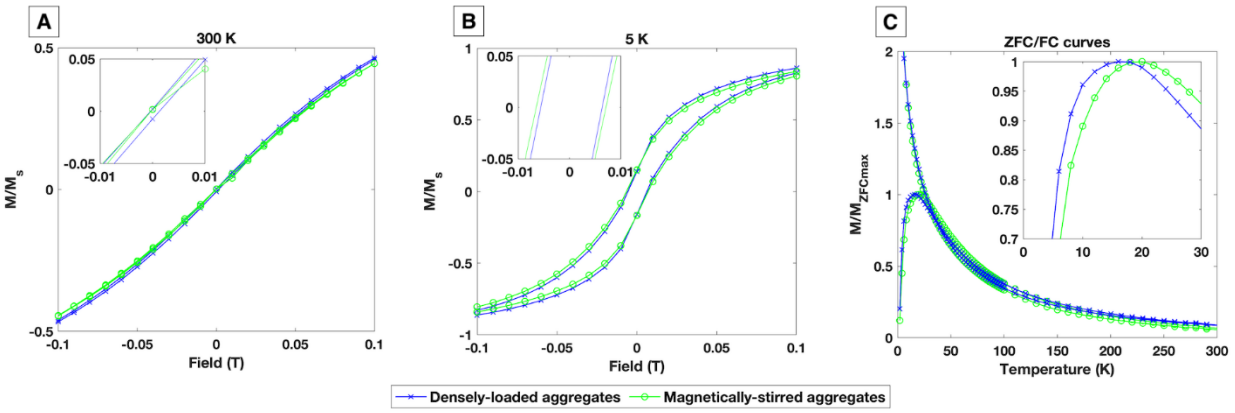

Supplementary Figure 9: Magnetization curves for densely-loaded aggregates (blue) and magnetically-stirred aggregates (green) at (A) 300 K field sweep -100 Oe < Field < 100 Oe, Inset: -0.1 T < Field < 0.1 T; (B) 5 K field sweep -100 Oe < Field < 100 Oe, Inset: -0.1 T < Field < 0.1 T; and (C) corresponding ZFC/FC curves measured at zero and 5T fields, respectively, Inset: 0-30 K.

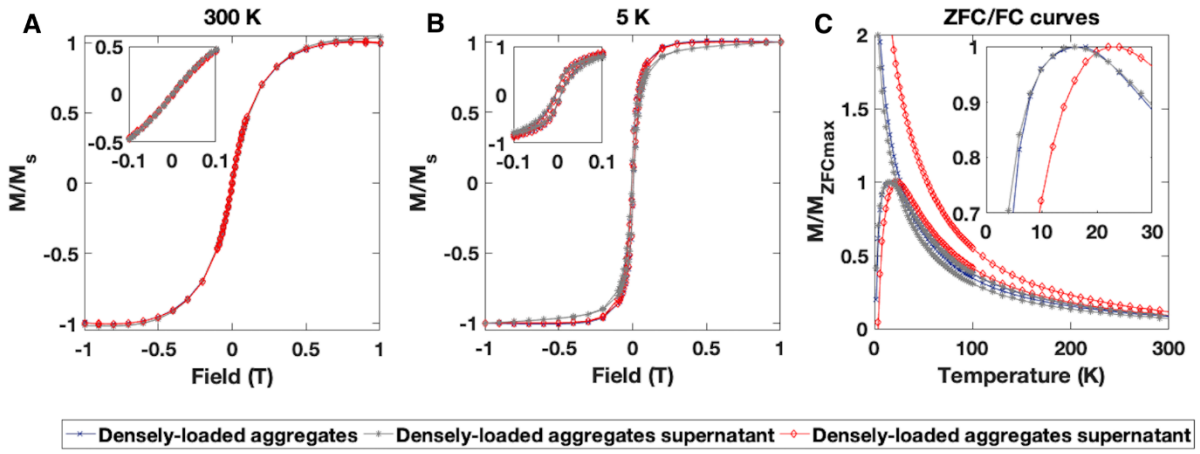

Supplementary Figure 10: Magnetization curves for densely-loaded aggregates (blue), pellets collected via magnetic exposure (red) and supernatant (gray) samples at (A) 300 K field sweep, Inset: -0.1 T < Field < 0.1 T; (B) 5 K field sweep, Inset: -0.1 T < Field < 0.1 T; and (C) corresponding ZFC/FC curves measured at zero and 5T fields, respectively, Inset: 0-30 K. Note that in A, B curves for densely-loaded aggregates and magnet-treated densely-loaded aggregates pellet and supernatant nearly completely overlap, obscuring the blue aggregate curve (magnified in Supplementary Figure 11).

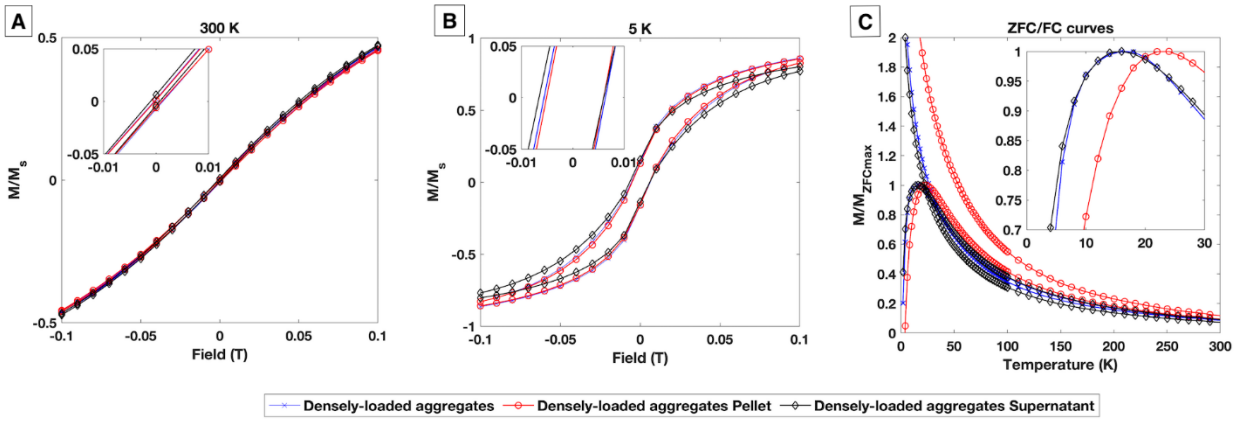

Supplementary Figure 11: Magnetization curves for densely-loaded aggregates (blue), pellets collected via magnetic exposure (red), and supernatant (black) samples at (A) 300 K field sweep -100 Oe < Field < 100 Oe, Inset: -0.1 T < Field < 0.1 T; (B) 5 K field sweep -100 Oe < Field < 100 Oe, Inset: -0.1 T < Field < 0.1 T; and (C) corresponding ZFC/FC curves measured at zero and 5T fields, respectively, Inset: 0-30 K.

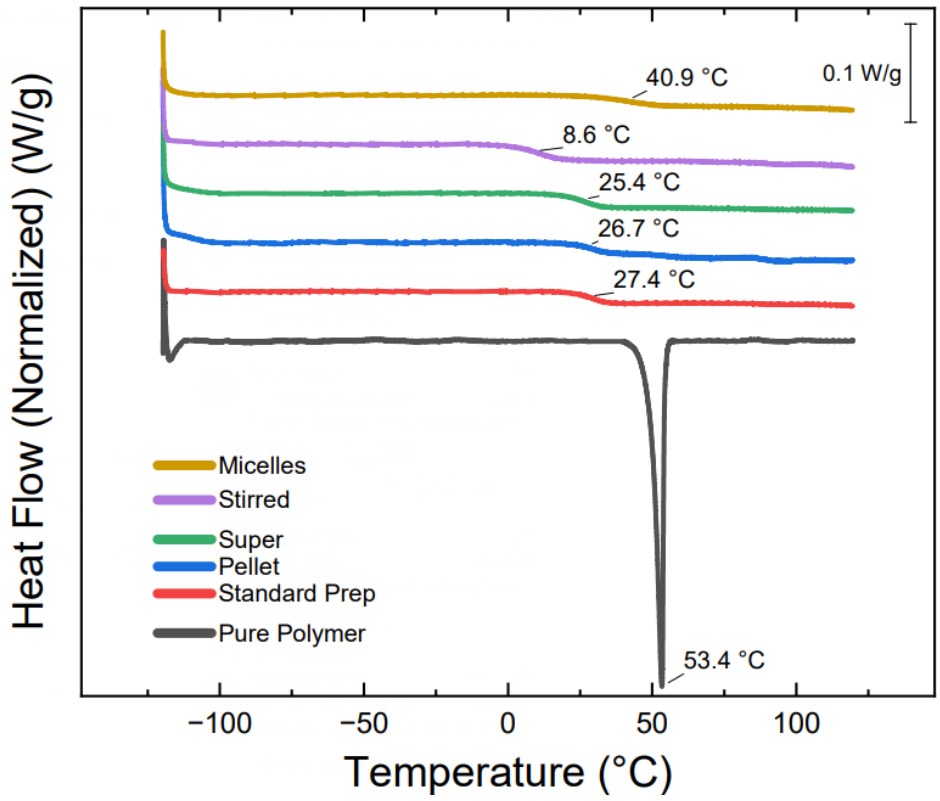

Supplementary Figure 12: Differential scanning calorimetry (DSC) curves.

Supplementary Table 1: Normalized standard deviation in the measurement fit of each sample for SQUID measurements.

Sample/Normalized Std. Dev	300K	5K	ZFC	FC
Dispersed, individual SPIONs	2.56E-04	1.09E-04	4.21E-05	9.58E-05
Densely loaded aggregates (SNC, no field)	8.38E-05	2.55E-05	7.99E-05	6.22E-05
Magnetically stirred densely loaded aggregates (SNC-St)	4.06E-04	1.62E-04	5.83E-05	8.48E-05
Magnetically concentrated Pellet (SNC-P)	6.78E-05	4.93E-05	2.39E-04	2.39E-04
Magnetically concentrated Supernatant (SNC-S)	7.31E-05	1.86E-04	3.43E-04	3.43E-04

References

(1) Nabar, G. M. Encapsulation of Nanoparticles and Polymers within Block Copolymer Micelles Prepared by the Emulsion and Solvent Evaporation Method. The Ohio State University, 2017.
(2) Kralj, S.; Makovec, D. Magnetic Assembly of Superparamagnetic Iron Oxide Nanoparticle Clusters into Nano chains and Nanobundles. *ACS Nano* **2015**, *9* (10), 9700-9707. DOI: 10.1021/acsnano.5b02328.
(3) Taepaiboon, P.; Rungsardthong, U.; Supaphol, P. Drug-loaded electrospun mats of poly(vinyl alcohol) fibres and their release characteristics of four model drugs. *Nanotechnology* **2006**, *17* (9), 2317-2329. DOI: 10.1088/0957-4484/17/9/041.